Two-Phase Xenon Time Projection Chambers for WIMP Searches and Other Applications

Nicole A. Larsen
Yale University Department of Physics
Advisor: Daniel McKinsey

Thesis Prospectus

May 24, 2012

Abstract

Astronomical evidence indicates that 23 % of the energy density in the universe is comprised of some form of non-standard, non-baryonic matter that has yet to be observed. One of the predominant theories is that dark matter consists of WIMPs (Weakly Interacting Massive Particles), so named because they do not interact electromagnetically or through the strong nuclear force. In direct dark matter detection experiments the goal is to look for evidence of collisions between WIMPs and other particles such as heavy nuclei. Here, the challenge is to measure exceedingly rare interactions with very high precision. In recent years xenon has risen as a medium for particle detection, exhibiting a number of desirable qualities that make it well-suited for direct WIMP searches. The LUX (Large Underground Xenon) experiment is a 350-kg xenon-based direct dark matter detection experiment currently deployed at the Homestake Mine in Lead, South Dakota, consisting of a two-phase (liquid/gas) xenon time projection chamber with a 100-kg fiducial mass. Its projected sensitivity for 300 days of underground data acquisition is a cross-section of 7×10^{-46} cm^2 for a WIMP mass of 100 GeV, representing an improvement of nearly an order of magnitude over previous WIMP-nucleon scattering cross-section limits.

Furthermore, two-phase xenon-based technologies are useful in many other applications, including other fundamental physics searches, imaging of special nuclear materials, and medical imaging. PIXeY (Particle Identification in Xenon at Yale) is a compact, multipurpose, liquid-xenon-based time projection chamber that operates in either single or two-phase (liquid/gas) mode. One of PIXeYs main goals is to explore the prospects for gamma-ray imaging with liquid xenon. Additionally, PIXeY will be used in particle discrimination studies and electron track studies which will be particularly useful for fundamental physics applications such as neutrinoless double-beta decay searches.

This prospectus gives an introduction to the LUX and PIXeY experiments, reports on the current status and discusses my specific involvement with each, and finally outlines the future prospects for LUX and for PIXeY.

1 Background

1.1 Missing Mass in the Universe

Perhaps the earliest indication of "missing mass" in the universe was presented by Fritz Zwicky in a famous 1933 paper concerning the velocity distribution of galaxies within the Coma Cluster. Using the Virial Theorem, Zwicky was able to calculate that, in order to obtain the abnormally large observed velocities of galaxies at the edge of the cluster, the mass density within the cluster would have to be approximately four hundred times larger than the density of luminous mass alone [1]. Zwicky coined the term "dark matter" to describe such non-luminous matter.

Subsequent studies of the dynamics of stars and galaxies have served only to reinforce the presence of dark matter. For example, the "timing argument", first set forth by Kahn and Woltjer [2], provides a method of estimating the mass of the galaxies in the Local Group based on their velocities with respect to each other. A spectral calculation for the Andromeda galaxy yields a velocity of approach of 125 km/s. Based on this velocity and considering only mass that is luminous, conservation of energy arguments show that the Andromeda-Milky Way system has net positive energy and therefore should be unstable. Kahn and Wolter estimated that an additional $1.5 \times 10^{12} M_\odot$ of unseen matter is necessary to keep the Local Group from flying apart. Additionally, some of the strongest dynamical evidence for the presence of dark matter in the universe comes from observations of the rotation curves of spiral galaxies. For a star near the outer radius of a galaxy, one expects the orbital velocity to decline as $1/r^2$ in accordance with Keplers laws. Rather, observations by Vera Rubin in the 1970s and 1980s showed that orbital velocities remain constant or decrease only slightly all the way out to the optical radius of the galaxy (Fig. 1). This is powerful evidence that the actual mass contained in galaxy extends far past the extent of the visible mass [3, 4].

The existence of dark matter is further supported by weak lensing. Gravitational lensing occurs when light is bent by the presence of a mass. In astronomy, this means that an overdensity in the foreground can distort the appearance of background structures. Non-luminous matter can therefore be observed by its effect on light from background galaxies [5]. Some of the most dramatic evidence for dark matter comes from observations of the cluster 1E0657558, commonly known at the Bullet Cluster. The Bullet Cluster consists of two smaller clusters that have undergone a merger. Images from the Chandra X-ray Telescope in conjunction with weak lensing data show clearly that the luminous mass, which consists primarily of hydrogen gas, is in a different location than the majority of mass in the cluster (Fig. 2). The most plausible explanation is that during the merger the gas in the two merging subclusters collided and interacted, creating drag, while the unseen mass in each subcluster passed through unimpeded [6].
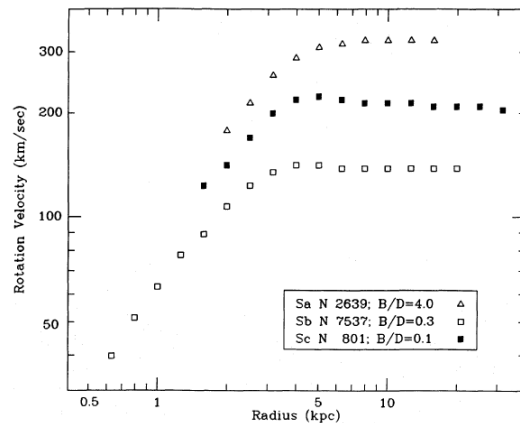

Figure 1: Rotation curves plotted for a type Sa, a type Sb, and a type Sc galaxy. Each type galaxy has a very different structure, yet the rotation curves show the same characteristic non-decreasing shape out to large radii [4].

A final class of evidence supporting the presence of dark matter comes from observations of the cosmic microwave background (CMB). Experiments such as WMAP [7] have produced detailed observations of this relic radiation that originated at the time of recombination, when the universe cooled to the point where photons could no longer ionize hydrogen atoms (T < 3000K). Today the CMB is at a remarkably uniform blackbody temperature of 2.7K. Anisotropies in the CMB power spectrum can be used to set constraints on fundamental parameters such as $\Omega_b \times h^2$, the baryon density in the universe, and $\Omega_m \times h^2$, the overall matter density in the universe, with the difference an indicator of nonbaryonic dark matter. Here, h represents the Hubble constant [8]. Similar limits on Ω_b can be obtained from observation of primordial abundances of light elements in the universe, which can be extrapolated from the abundances of these same elements in the universe today [9].
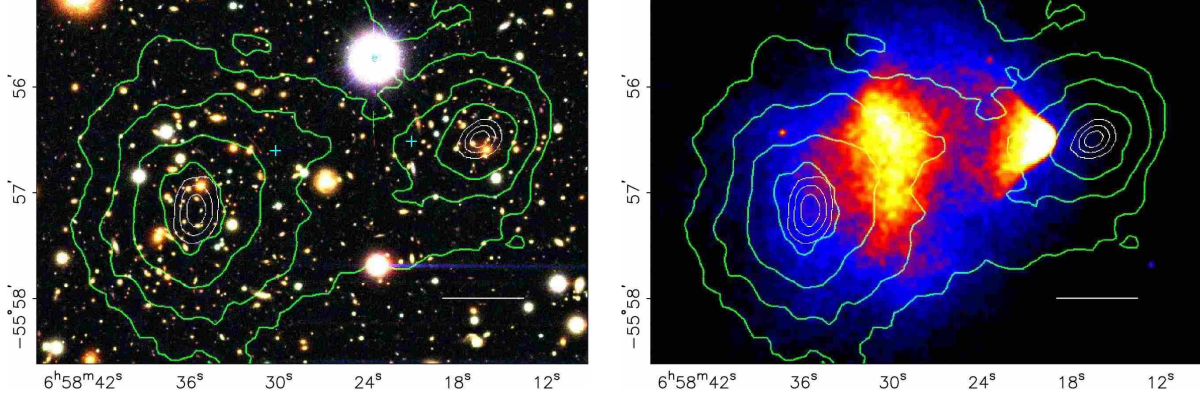
1

Figure 2: Cluster 1E0657-588, shown on the left as a color image from the Magellan telescope and on the right as an image from the Chandra x-ray telescope. The green contours indicate the mass distribution in the cluster determined from weak lensing observations. The visible matter is localized in a different area than the bulk mass, suggesting the presence of unseen matter [6].

Each of these pieces of evidence is consistent with the others, and moreover they all appear to be consistent with a cosmological model comprised of the following constituents in the following proportions [7]:

$$\Omega_b = 0.0456 \pm 0.0016$$
$$\Omega_{dm} = 0.227 \pm 0.014$$
$$\Omega_\Lambda = 0.728^{+0.015}_{-0.016}$$

Here Ω_b is the baryon density, Ω_{dm} the dark matter density, and Ω_Λ the dark energy density in the universe (Fig. 3).

1.2 Dark Matter Candidates

In the past seventy years, many solutions to the dark matter problem have been proposed. The first and least exotic possibility is that dark matter consists of ordinary baryonic matter which is simply too dim to be observed. Examples of such objects, called Massive Compact Halo Objects (MACHOs), include black holes, neutron stars, brown dwarfs, or planets. However, as previously mentioned, Ω_b is constrained from observations of the CMB and from big bang nucleosynthesis to be much less than Ω_m, ruling out MACHOs as more than a small component of the dark matter [8, 9]. Neutrinos have also been largely rejected as a dark matter candidate, since relativistic dark matter, also known as "hot dark matter", tends to smooth out fluctuations in the early universe and thus suppress structure formation [11]. Large scale surveys such as the Sloan Digital Sky Survey have helped place constraints both on the mass of the neutrino and on the fraction of dark matter that could be comprised of neutrinos [12].

One of the best-motivated candidate dark matter particles is the Weakly Interacting Massive Particle, or WIMP. WIMPs are thought to be thermal relics from the Big Bang.
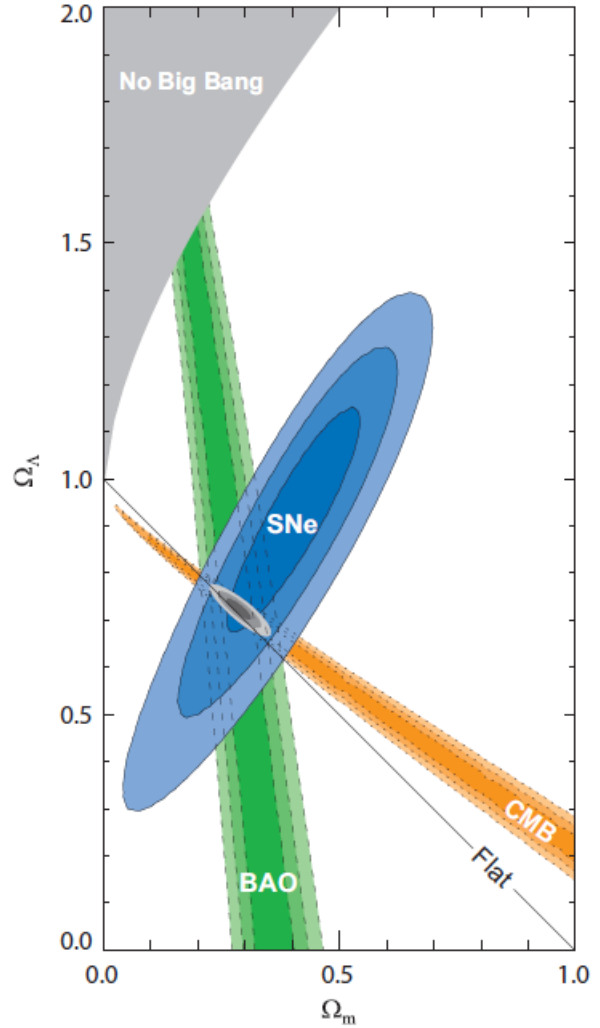

Figure 3: Constraints on Ω_m and Ω_Λ from CMB, baryon acoustic oscillations, and supernova data [10].

2

Such particles would have been initially present in large amounts, continuously creating and annihilating, but then would have "frozen out" as the universe expanded and cooled, leaving behind a "relic" density. For electrically neutral particles with masses in the range of tens to thousands of GeV, having an annihilation cross-section on the scale of the weak interaction $< \sigma_a v > \sim 10^{-25}$ cm^2 leads to dark matter densities of the same order of magnitude as the measured Ω_{dm}. Examples of possible WIMP candidates include neutralinos, which are light supersymmetric particle of gauge bosons, and light neutral states in the Higgs sector [13]. The experiments detailed in this prospectus focus on the hunt for WIMPs.

A viable alternative to the WIMP hypothesis is the axion, which is a light (μeV to meV) spin-0 boson first postulated as a solution to the strong CP problem in particle physics. Its weak coupling to photons makes it possible to be observed via $a \to \gamma\gamma$ interactions. For a review of axion physics, see [14].

Finally, Modified Newtonian Dynamics (MOND) theories seek to provide an alternative solution to the dark matter problem through corrections to Newton's second law and to the $1/r^2$ dependence of gravitational force. MOND was first proposed by Mordehai Milgrom as an alternative explanation for the rotation curves of galaxies. Here, it met with a good deal of success [15, 16]. On the other hand, weak lensing observations such as the Bullet Cluster tend to disfavor MOND theories.

1.3 Direct WIMP Detection

There are three main categories of WIMP experiments. First, direct detection experiments seek to observe recoils between incident WIMPs and target nuclei. Such events are rare, due to the weak scale of the cross-sections, but should still occur occasionally due to the Earth's motion through the galaxy's dark matter halo. Secondly, indirect detection experiments look for annihilation products from dark matter interactions. Examples of such experiments include the FERMI satellite, which looks for gamma-ray signals and excesses of electrons and positrons at the TeV and sub-TeV scale in cosmic rays, and ICECUBE, which looks for neutrinos produced by WIMP annihilations [17]. Finally, WIMPs could be produced in accelerator experiments such as the Large Hadron Collider at CERN.

In direct dark matter searches, there are a few different methods by which one can observe WIMP-nucleon recoils. First, one can look for annual modulation in signals above a constant background occurring due to the Earth's motion around the sun as it travels through the Milky Way's dark matter halo. DAMA/LIBRA is an example of such an experiment [18]. Alternately, an experiment can look for energy transfered in collisions between WIMPs and a target material. This energy is typically deposited into three different channels: it can be deposited in the form of scintillation light, ionization charge, or in the form of phonons. The Large Underground Xenon (LUX) experiment, which is a primary focus of this prospectus, looks for energy deposited in the form of scintillation or charge. In contrast, an example of an experiment that uses the phonon channel is the CDMS experiment, which searches for very small temperature changes due to WIMP recoils in ultra-pure germanium crystal targets [19].

For each of these channels, the recoil energy spectrum of a WIMP off of a target nucleus is expected to be smooth and monotonically decreasing, with the basic form:

$$\frac{dR}{dE_R} = \frac{R_0}{E_0 r} \exp\left(\frac{-E_R}{E_0 r}\right) \times F^2(E_R) \times I$$

Here R is the rate per unit mass, E_R is the recoil energy, R_0 is the total event rate, E_0 is the most probable incident kinetic energy, and $r = 4 \times (M_\chi M_A)(M_\chi + M_A)^{-2}$ is a kinematic factor involving the mass of the target nucleus A and the mass of the incoming WIMP χ. F^2 and I include corrections due to the Earth's motion around the sun, instrument resolution and threshold effects, and nuclear form factors that take into account the size of the target nucleus whether the interaction is spin-independent or spin-dependent. For a WIMP of mass 10 GeV 1 TeV, typical recoil energies are in the range of 1-100 keV [20]. The main challenges in these direct detection experiments are to reduce backgrounds and to achieve sufficient energy resolution and thresholds to detect low-energy recoil signals.
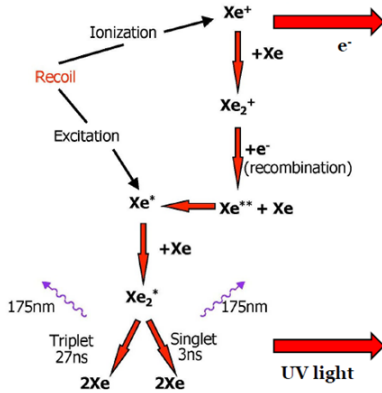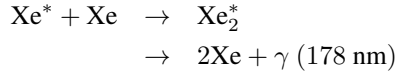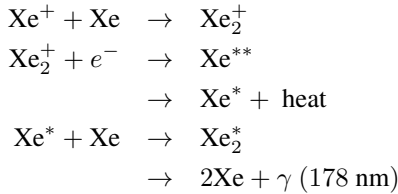
1.4 Xenon as a Medium for WIMP Detection

Figure 4: Charge and light production in xenon caused by interaction with an incident particle.

Xenon is a particularly attractive WIMP target for a number of reasons. First, its high density (3 g/cm^3) and high atomic number (z=54) increase the total probability of interaction, while the relative abundance of odd isotopes such as ^{129}Xe and^{131}Xe allow for the possibility of detecting spin-dependent interactions. Secondly, it has a high scintillation and ionization yield, allowing for detection of recoils at low energies. Third, xenon has no long-lived radioactive isotopes, making it advantageous over other noble elements for low-background experiments. Its longest-lived isotope is ^{127}Xe with a half-life of 36 days. In contrast, argon, which is used in for example the DEAP/CLEAN dark matter search, has a large abundance of ^{39}Ar with a half-life of 268 years [21]. Lastly, xenon is far more reasonably priced ($1000/kg) than many target materials such as germanium ($20,000/kg) or CZT ($50,000/kg) used in other WIMP searches.

When an incident particle interacts with a xenon atom inside a detector, it will either excite or ionize the xenon. In each case, the xenon atom will form an excited di-mer with one of the surrounding xenon atoms, and this molecule when it de-excites will give off scintillation light at a wavelength of 178 nm. The exact mechanism is shown in Fig. 4 and outlined in more detail below [22].

For excitation:

$$
\begin{aligned}
\mathrm{Xe}^* + \mathrm{Xe} \quad &\rightarrow \quad \mathrm{Xe}_2^* \\
&\rightarrow \quad 2\mathrm{Xe} + \gamma \,(178 \text{ nm})
\end{aligned}
$$

For ionization:

$$
\begin{aligned}
\mathrm{Xe}^+ + \mathrm{Xe} \quad &\rightarrow \quad \mathrm{Xe}_2^+ \\
\mathrm{Xe}_2^+ + e^- \quad &\rightarrow \quad \mathrm{Xe}^{**} \\
&\rightarrow \quad \mathrm{Xe}^* + \text{ heat} \\
\mathrm{Xe}^* + \mathrm{Xe} \quad &\rightarrow \quad \mathrm{Xe}_2^* \\
&\rightarrow \quad 2\mathrm{Xe} + \gamma \,(178 \text{ nm})
\end{aligned}
$$

In both cases we refer to this scintillation light as "prompt" or "S1" scintillation. In the case of ionization, the free charge can be drifted by an applied electric field, preventing recombination and thus partitioning the deposited energy into a light signal and a charge signal. In a two-phase xenon time projection chamber such as LUX, XENON, which is another xenon-based direct WIMP search experiment [23], or EXO, a xenon-based double-beta decay search [24], the charge signal is read out by drifting the free electrons upwards toward the liquid-gas interface (Fig. 5). Once the electrons approach the liquid-gas surface, they can be accelerated into the gaseous phase by applying an extraction field on the order of 10 kV/cm. The electrons then accelerate rapidly through the gas, striking xenon atoms and causing them to fluoresce before being accelerated again by the extraction field. This secondary signal is called "proportional" scintillation, because it is proportional to the amount of charge produced in the initial interaction, or "S2" scintillation.

The "charge-to-light" or S2/S1 ratio provides a powerful tool for discriminating between electronic recoils (e.g. gammas , electrons) and nuclear recoils (WIMPs, neutrons, alpha particles) inside a detector. Electronic events tend to have a much higher S2/S1 ratio than nuclear recoils. In Fig. 6, data from a calibration performed by the XENON collaboration shows clear separation between neutron and gamma bands [23]. The remaining backgrounds are neutrons, which mimic WIMPs inside the detector, and some leakage from low-energy gamma events. To date, the highest discrimination reached by this method is a 99.99% rejection of electronic events, achieved by the ZEPLIN-III experiment during their first science run in 2009 [25].
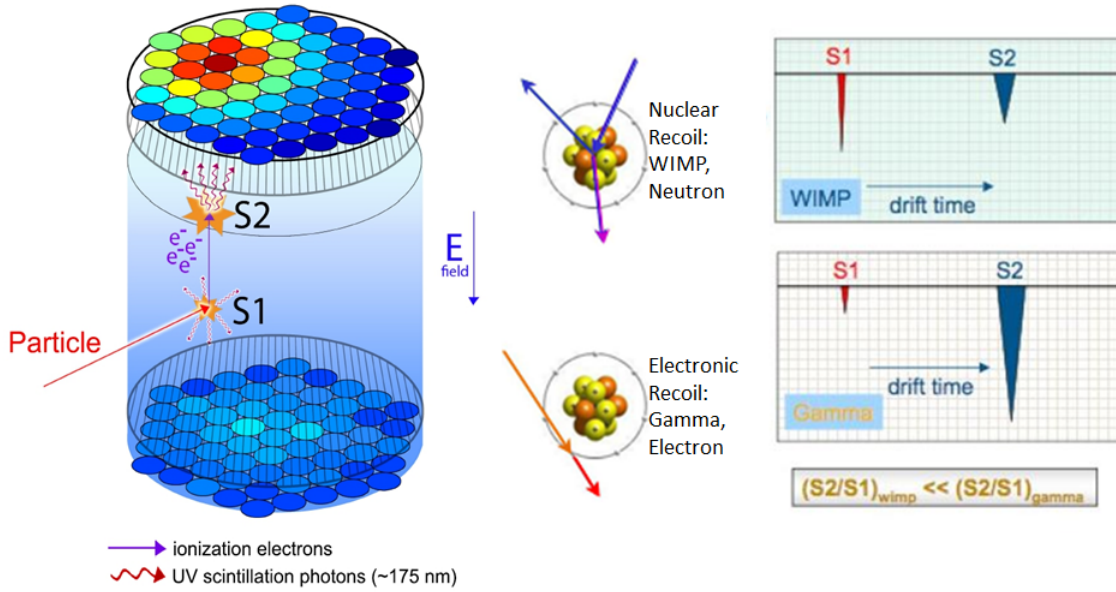
Figure 5: Principle of operation for two-phase xenon time projection chambers.

One final advantage of xenon over other target materials is its self-shielding ability. At low energies gammas interact primarily with xenon atoms through photoelectric absorption. The mean free path of gammas in xenon is very short (3 mm for 122 keV), so that low-energy gammas are stopped at the edges of the detector [22]. By careful choice of fiducial volume and rejection of multiple scatters, one can almost entirely eliminate backgrounds from external gammas and from surface radioactivity inside the detector.

Figure 6: S2/S1 vs. energy for elecronic (black) and nuclear recoils (red) during calibration of the XENON10 detector. During this experiment 99.5% discrimination between electron and nuclear recoils was achieved. [23].

2 The Large Underground Xenon (LUX) Experiment

LUX is a two-phase xenon-based WIMP detection experiment deployed at the Homestake Mine in Lead, SD. The collaboration consists of 90 scientists from 15 different member institutions around the world. In February 2012, LUX completed its second surface run with the goal of fully testing all systems in preparation for underground deployment on the 4850' level of the Homestake Mine, where it will begin its first science run at the end of 2012. The projected sensitivity after 300 days of underground science operations is 7×10^{-46} cm^2, nearly an order of magnitude better than the current cross-section limit established by the XENON100 experiment, making it the most sensitive WIMP detector in the world.

2.1 Design

The LUX detector consists of 350 kg of xenon, with a 300-kg active volume and a 100-kg fiducial volume housed inside two concentric ultra-radiopure titanium cryostats. The xenon is observed by two arrays containing a total of 122 Hamamatsu R8778 photomultiplier tubes (PMTs) located on the top and the bottom of the main volume, which is lined with reflective PTFE panels to increase light collection. Immediately inside the PMT arrays is a set of wire grids that produce the drift and extraction fields inside the detector. The detector is cooled to liquid xenon temperature (180 K)
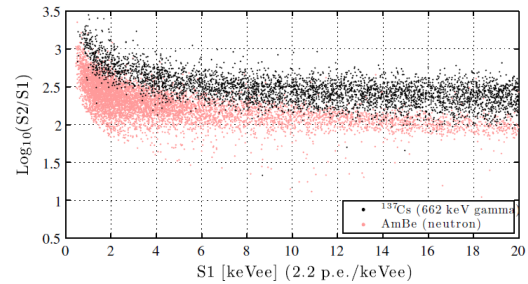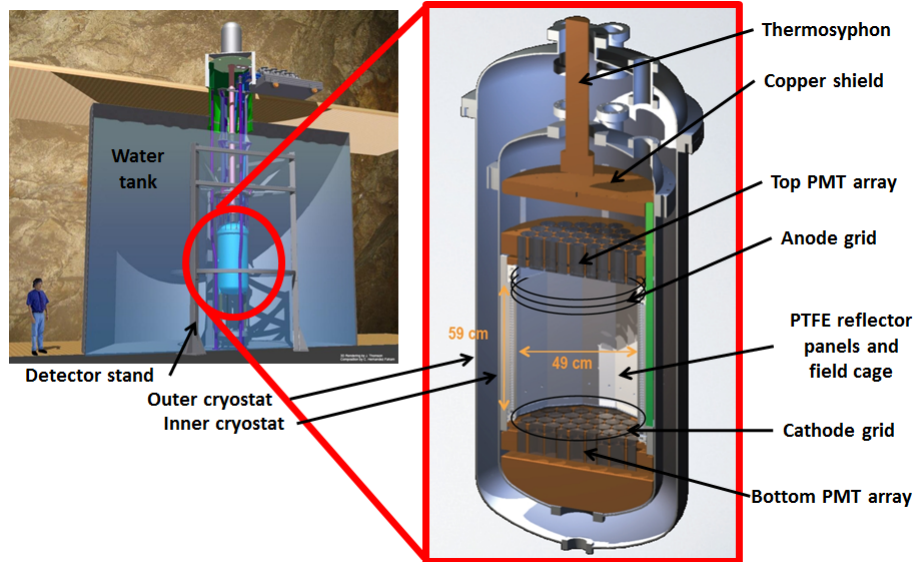
Figure 7: Schematic of the LUX detector.

by a novel cryogenic system with four thermosyphons, each consisting of a closed loop of nitrogen that continuously evaporates and condenses, drawing heat from the main volume (Fig. 7).

LUX employs an number of tricks for reducing backgrounds due to cosmogenic flux, ambient radioactivity, and radioactivity inside the detector. First, the Davis Campus at Homestake where LUX will be situated is 4850' underground. This reduces cosmic ray flux by a factor of 10^7. Secondly, deployment into a 300-ton water tank suppresses gammas by a factor of 10^7 and neutron backgrounds by factors of 10^3 and 10^9 for high-energy (>10 MeV) and low-energy neutron, respectively. Next, careful fiducial cuts are made and multiple scatters rejected to further reduce background from gammas and surface radioactivity (Fig. 8). Last, precautions are taken to limit the internal background. When the detector is open, the internals are under a continuous N_2 purge to limit Rn deposition, and Kr is removed using a charcoal column. All detector materials are carefully counted to ensure adherence to a strict radioactivity budget.

The PMTs used in LUX are extremely low radioactivity, specially designed for low-background physics in a collaborative effort between Hamamatsu and the XMASS and LUX collaborations. They have < 9.5 mBq ^{238}U, < 2.7 mBq ^{232}Th, and < 66 mBq ^{40}K per PMT. They perform extremely well at cryogenic temperatures and are able to efficiently detect 178-nm scintillation light, rendering it unnecessary to dope the xenon with a wavelength shifter.
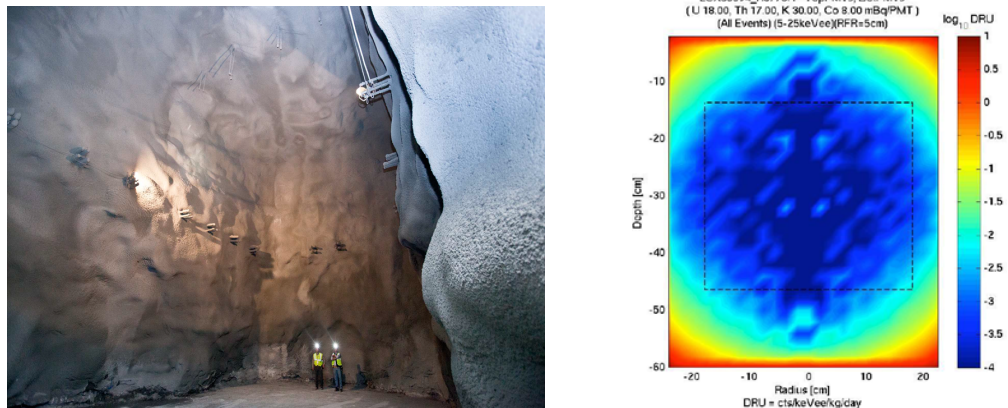

Figure 8: (Left) The underground site of the LUX detector, in the Davis Cavern at Homestake Mine in South Dakota. (Right) Simulated gamma backgrounds vs. radius for the LUX detector, showing the effectiveness of self-shielding.

6

With regards to performance, the PMTs have a 33% quantum efficiency and 90% collection efficiency for an approximate 30% overall efficiency. During Run 02 the PMTs were operated at a gain of approximately 3×10^6. 121/122 PMTs were fully operational during Run 02 (Fig. 9).
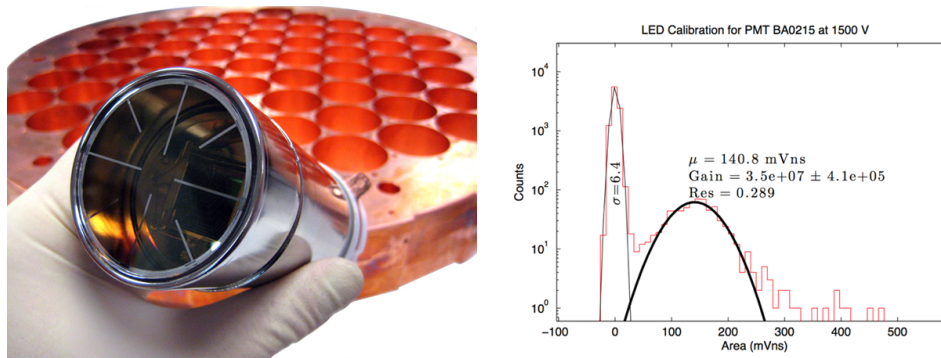

Figure 9: (Left) A photograph of the LUX Hamamatsu R8778 PMTs and the copper block that houses them. (Right) A gain calibration performed using single photo-electron measurements from one of the PMTs.

The gas-handling system for LUX includes an SAES MonoTorr external heated metal purifier, KNF diaphragm pumps for circulating xenon through the purifier, a compressor for recovery of the xenon into storage bottles, along with all associated plumbing, instrumentation, and safety devices. It includes also a storage vessel and an in-situ cold-trap/RGA analysis system, sensitive to 0.7 ppb O_2 mol / mol and 0.5 ppt Kr mol / mol [26]. The LUX system is able to circulate up to 35 SLPM through the external purifier, corresponding to a complete turnover in 1.2 days of all of the xenon in the detector, with stable temperature control provided by the thermosyphon cooling system and 98% efficient heat exchange with a two-phase heat exchanger. During Run 02 the electron lifetime was monitored by muon, alpha, and gamma signals (Fig. 10).

The high voltage in the cathode needed to produce the drift field in the detector is supplied by an external Spellman power supply and routed into the detector via a Heinzinger 100-kV rated cable that must be fed through from outside the detector into the xenon space. For Run 02, a fluted ceramic feedthrough ultra-high-vacuum produced by Ceramtec was used. Due to radioactivity concerns, this feedthrough is located far away from the main volume at the end of a meters-long conduit. The operating voltage is limited by the breakdown voltage in warm gaseous xenon near the feedthrough. The Ceramtec feedthrough has been tested up to 25 kV total and was biased up to a maximum of 10.3 kV during Run 02. A safe operating voltage was determined to be 7.5 kV, corresponding to a drift field of 300 V/cm.

A novel feedthough design has since been developed using StyCast 2850 Blue aluminized epoxy. This epoxy is a very good insulator, with good thermal conductivity and a low coefficient of thermal expansion. In the new feedthrough design, the StyCast is used to form a vacuum seal to the unbroken Heinzinger cable. This design has been tested up to 100 kV for four weeks and is currently installed in the detector. Additionally, a spare is under construction at Yale (Fig. 11).

Finally, the LUX calibration system consists of a number of acrylic tubes located outside the detector, enabling the deployment of sources next to the detector inside the water tank (Fig. 12). Additionally, a set of sources such as Rn and ^{83m}Kr can be internally doped into the detector to provide full coverage of the entire internal volume. During Run 02 a number of calibrations were successfully performed using external sources (Fig. 13).

2.2   Summary of Run 02 Performance and Current Status

During Run 02, all systems were fully tested. We demonstrated the successful deployment of the the detector into a surface water tank shield. The PMTs, trigger, and DAQ systems all work, with an excellent light yield. Additionally, stable cryogenic control was achieved for over 100 days of running. Finally, xenon was successfully recovered to a storage vessel by cryopumping.
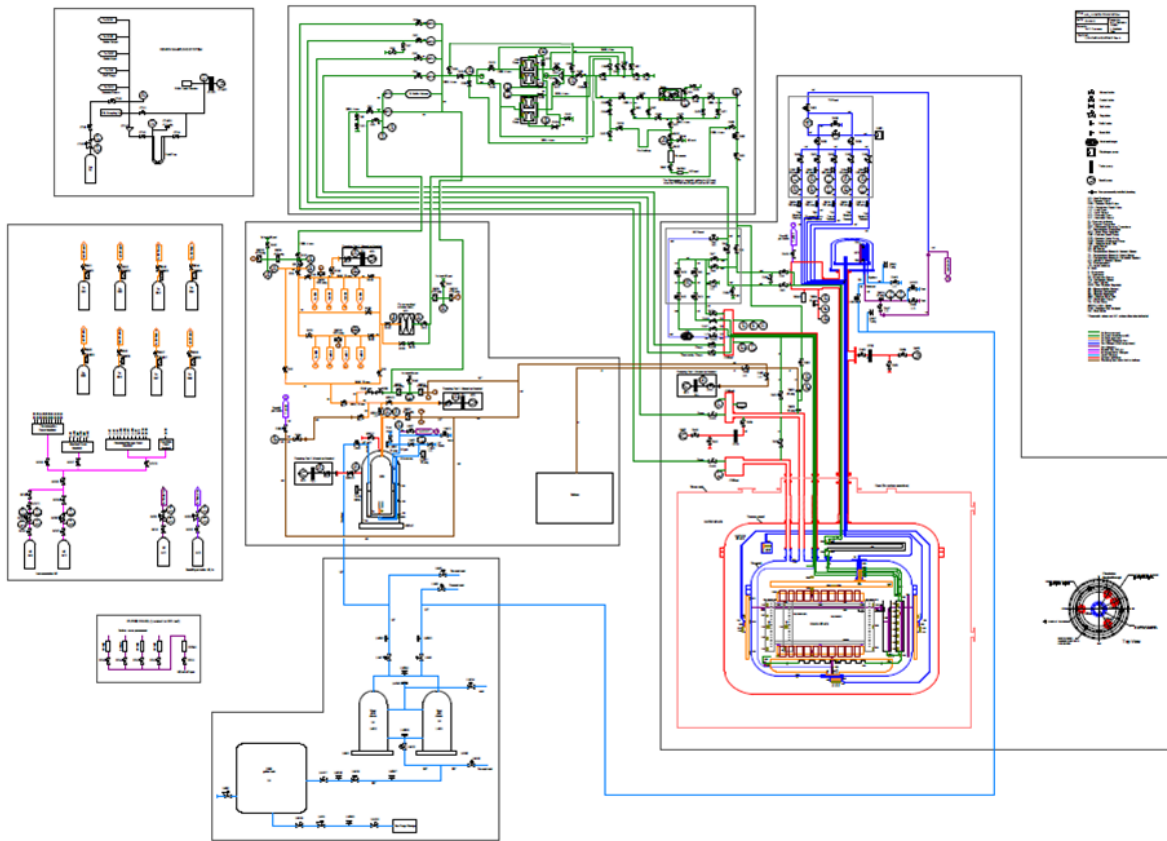
Figure 10: A schematic of the LUX gas handling system. Red lines indicate plumbing associated with the main detector, dark blue the thermosyphon system, light blue the LN_2 system, green the main circulation panels, and orange the high pressure plumbing associated with the storage cyinders and the Storage and Recovery Vessel (SRV).
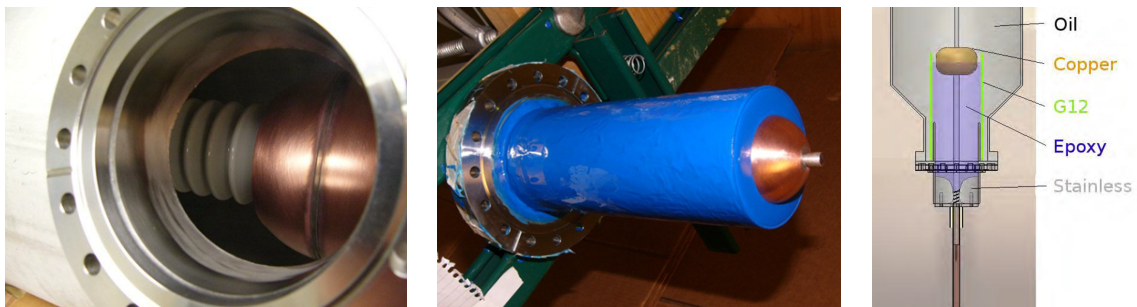

Figure 11: (Left) Photograph of the original Ceramtec cathode high voltage feedthrough, installed. (Center) Photograph and (right) schematic of the epoxy feedthrough.

The maximum electron lifetime achieved during the surface run was 90 μs. This was significantly shorter than the lifetime corresponding to the full length of the detector (500 μs). The drift time was limited by inefficient mixing of purified xenon into the main volume caused by a disconnect in internal plumbing, which has since been repaired.

The drift field was limited to 300 V/cm during Run 02. We anticipate higher drift fields during the science run due in part to the cathode high voltage upgrade discussed in the previous section, which has already been installed.

2.3   Specific Involvement

I first became a member of the LUX collaboration in June 2010, and in accordance with collaboration publication policy I joined the author list in June 2011. From 2010 to present, I have traveled to Homestake six times and spent a total of 135 days on site. I have been involved with the following aspects of LUX design, construction, and operation:

1. CeramTec feedthrough installation
2. Detector deployment into surface water tank
3. Circulation system

   - Plumbing design and installation
   - Instrumentation rewiring
   - Maintenance of circulation pumps
   - Flow calibration

4. Xenon gas tracking and inventory
5. Epoxy feedthrough construction and testing (at Yale)
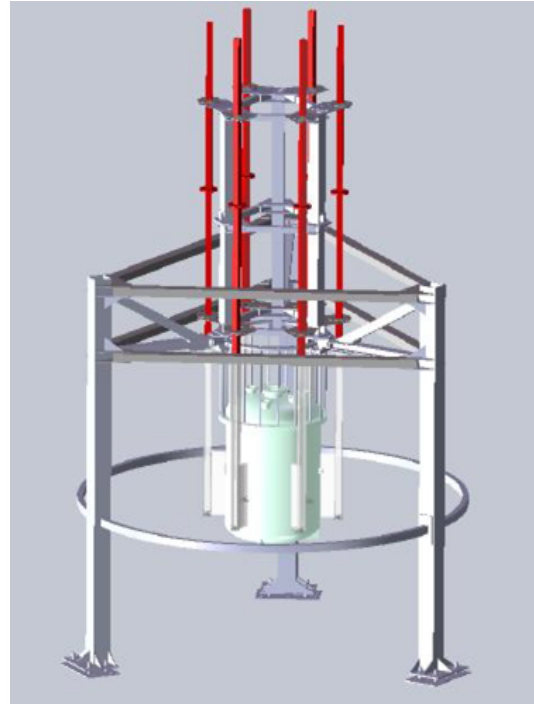6. Detector operations during Run 02

Figure 12: Schematic of the LUX calibration system. Source deployment tubes are indicated in red.

Additionally, in November 2011, I served as Shift Manager, coordinating all on-site activities, writing daily activity reports, and serving as liaison between the LUX crew and Sanford Laboratory at Homestake.

Finally, I have presented my work on LUX in the following arenas:

1. April APS Meeting 2012 (Oral)
2. DarkAttack 2012 (Poster; upcoming in July)
3. Presented results at three LUX collaboration meetings (Oral)
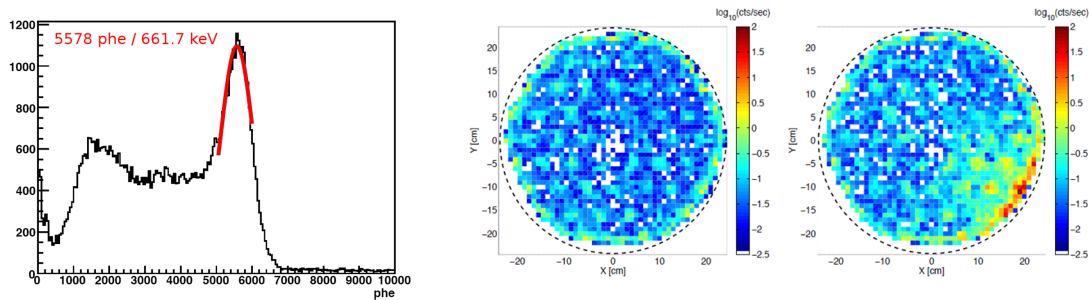4. Yale Department of Physics Grad Student Lunch Talk March 2012

Figure 13: (Left) Data from a calibration with a ^{137}Cs source, showing clearly a photopeak at 662 keV. These calibrations allow us to calculate our light yield, in this case 8 photo-electrons per keV. (Right) A first attempt at position reconstruction using a ^{137}Cs source. The left plot is background data, while the right plot contains data taken in the presence of the source.

2.4 Future Plans

Currently, LUX is undergoing a few small upgrades and being prepared for underground deployment in the Davis Cavern at Homestake, 4850 feet underground. The underground move will take place during Summer and Fall 2012, with the goal of beginning the first science run (Run 03) by the end of 2012. Finally, in mid-2014, LUX will begin its second science run. Again, 300 days of data collection is projected to yield a sensitivity of 7×10^{46} cm^2 (at 100 GeV), approximately one order of magnitude better than the current best limit (Fig. 14). Additionally, there are a number of other physics analyses that will be done. LUX is sensitive to spin-dependent interactions and will be capable of setting a limit on spin-dependent WIMP cross-section. LUX data can also be used to search for exotic WIMPs such as Kaluza-Klein particles, or to search for light (<10 MeV) WIMPs. Regarding the latter, a number of performance studies such as light collection and threshold effects will also need to be performed.
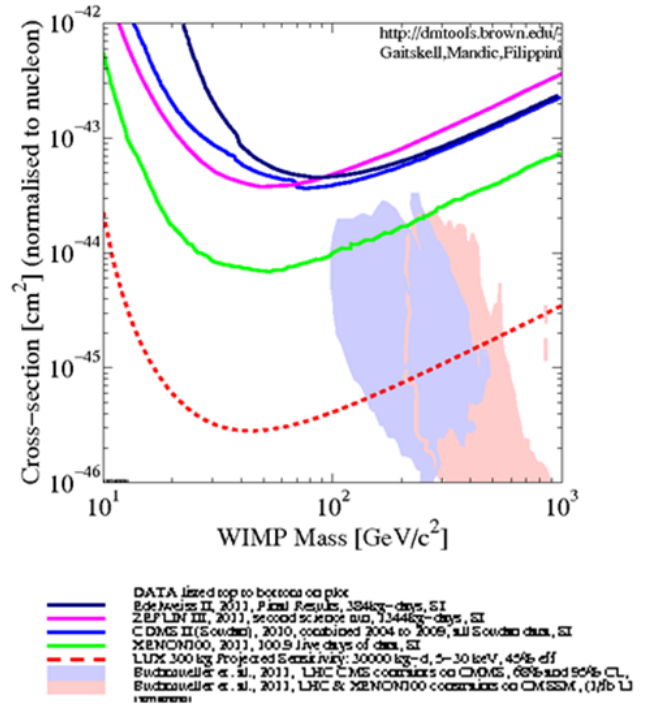
Figure 14: Experimental limits on WIMP cross-section vs. mass. The green line is a result produced by XENON100 representing the current best sensitivity limit. The red dashed line represents LUX's projected sensitivity.

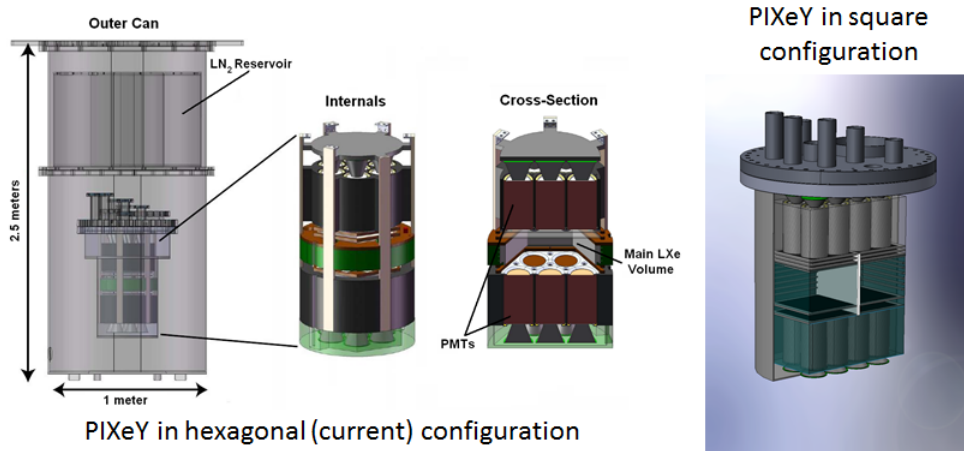Figure 15: The LUX collaboration, March 2012.

Figure 16: A schematic of the PIXeY detector in each of its two possible configurations.

3 Particle Identification in Xenon at Yale (PIXeY)

PIXeY is a small-scale xenon-based time projection chamber located at Yale University. The project represents a collaborative effort between Yale and University of Connecticut and consists of a dozen scientists from both institutions. PIXeY operates in either single (liquid) or two-phase (liquid/gas) modes. Its advantages include a high signal-to-noise ratio, low false alarm rates, and efficient collection of and discrimination between gamma rays and neutrons. PIXeY's purpose is multifold: to explore the prospects for Compton gamma-ray imaging with liquid xenon, to study the effect of electric field on discrimination power, and to perform electron-track studies for use in neutrinoless double-beta decay searches (Fig. 16).

3.1 Compton Imaging Overview

Compton imaging with PIXeY works as follows: The detector is mechnically divided into different optical modules. Each region is separated from the others by a thin, reflective PTFE wall. We are primarily concerned with events where an incident gamma ray scatters in one module and is photo-absorbed in another. A single-wire charge readout will allow very good (sub-mm) xy-position resolution, while timing between the prompt scintillation and the charge signal will provide the z-position. The energy is determined from the total size of the signals. The angle of incidence of the incoming gamma ray is then determined by the following equation for Compton scattering:

$$\phi = \arccos\left[1 - m_e c^2 \left(\frac{1}{E_2} - \frac{1}{E_1 + E_2}\right)\right]$$

Here, ϕ is the the angle of incidence, m_e the electron mass, E_1 the energy deposited in the initial scatter, and E_2 the energy deposited when the gamma is photo-absorbed. The value of ϕ determines a "cone of origin" for the gamma ray. In order to differentiate a source from background gammas, we search for overlap between cones corresponding to several different gammas. This intersection would indicate the likely presence of a gamma source. Such a technology could be used for the detection and imaging of special nuclear materials.

As an aside, information can also be gleaned from gamma rays that scatter and photo-absorb in the same optical module. Additionally, information can be gained for gammas that scatter more than once inside the detector. However, the position and energy reconstruction become more complicated in these latter cases, and events consisting of a scatter in one module and an absorption in another occur with high enough frequency that events with multiple scatters or scatter/absorption in the same volume can in general be discarded.

This technology has many uses; in particular it could be used for Homeland Security applications such as cargo inspection (Fig. 17).
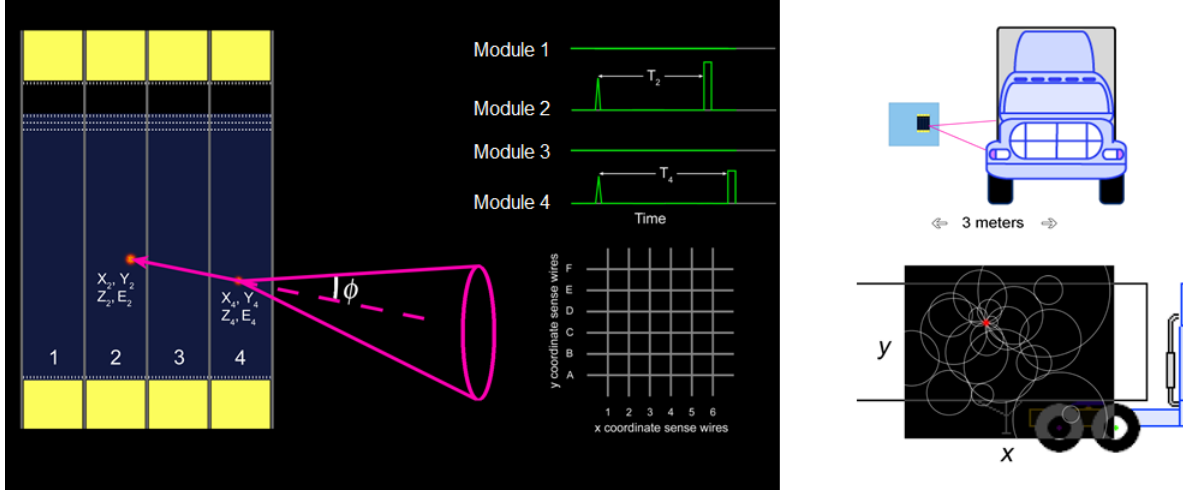
Figure 17: The Compton imaging concept. A gamma ray scatters in one optical module and photo-absorbs in another. Charge-sensing wires give a high xy-position resolution, while drift times give the precise z-position of each event. A "cone of incidence" can then be reconstructed, and, if there is an intersection of many cones, the presence of a nearby gamma source can be inferred with great accuracy.

3.2 Design and Performance Goals

PIXeY has many of the same design components as LUX, with a few notable differences. PIXeY has two different design configurations. In its current conficuration, a fiducial volume of approximately one liter is viewed on top and bottom by two arrays of seven PMTs each. Like LUX, a drift field is supplied by wire grids on the top and bottom of the main volume, with a set of field rings to keep the field constant, and it is walled by a set of reflective teflon panels to ensure as much light collection as possible. This "hexagonal" configuration is used primarily for R&D and testing. In the second configuration, PIXeY will have arrays of nine PMTs on the top and on the bottom. This "square" configuration will be divided into optical volumes for Compton imaging.
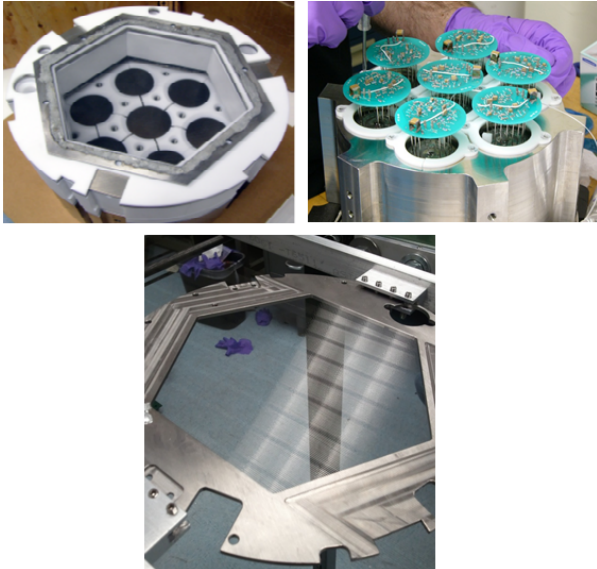

Figure 18: (Top left) The main volume of PIXeY before installation, including the anode grid, PMT block, and reflective PTFE panels. (Top right) Installation of the PIXeY top PMT array. (Bottom) A wire field grid under construction.

Energy resolution is crucial for Compton imaging, as the energy resolution of the detector directly affects the angular resolution with which a source can be located. The best energy resolution achieved by two-phase xenon-based technology to date is 5.9% full-width half maximum (FWHM) at an energy of 662 keV, obtained by the XENON10 experiment [23]. For single-phase xenon time projection chambers, the current best limit is 10.6% FWHM at 2615 keV, obtained by the Enriched Xenon Observatory (EXO), which searches for neutrinoless double beta decay in ^{136}Xe [24]. In comparison, PIXeY's projected energy resolution is 2.6% FWHM.

There are a number of design aspects that will help PIXeY to achieve this resolution. First, PIXeY uses the same Hamamatsu R8778 PMTs that are used in LUX, with excellent light collection and a quantum efficiency of 33%. Additionally, we have developed a set of parallel wire grids that allow the separate tuning of the electric fields in the liquid and in the gaseous region of the detector in order to optimize energy resolution. The grids have also been optimized for field uniformity and for light collection, with a highly uniform wire tension and an optical transparency of 92% (Fig. 18).
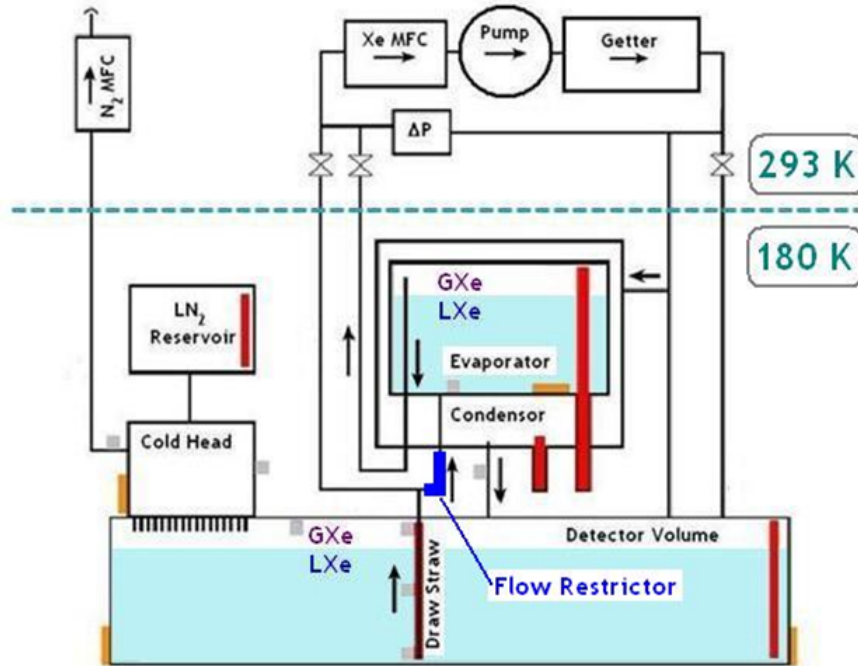
Figure 19: A schematic of the PIXeY circulation system.

These wire grids will also allow us to study the effect of electric field on particle discrimination. To date, the best discrimination between electron and nuclear recoils to be achieved with a xenon-based WIMP search is 99.99%, produced by the ZEPLIN-III experiment during their first science run. During this run, the detector operated at an extremely high drift field of 3.9 kV/cm [25]. So far, no dedicated studies have been performed to determine the extent to which the electric field contributed to the discrimination power in this experiment. PIXeY will be able to explore discrimination at fields of up to 8 kV/cm.

One final goal of PIXeY is to explore track shape discrimination in order to discriminate between gammas and betas. This is a novel idea which will be especially useful in double-beta decay searches. A gamma ray incident inside of the detector will theoretically deposit most of its energy at the end of its track, while the back-to-back betas ejected in double-beta decay should exhibit two tracks, each one with the bulk of the energy deposited at the end. The two kinds of events should exhibit differences in the S2 signal that they produce, allowing for potentially very good discrimination between beta decays and background

Figure 20: (Left) The PIXeY detector, fully installed, showing the position of the PIXeY two-phase heat exchanger. (Top right) A close up of the heat exchanger. (Bottom right) The heat exchanger, opened up and taken apart to show separately the inner copper pot (evaporator) and the outer steel cryostat (condenser).

gammas. This track shape discrimination could also be useful in determining the directionality of an incoming gamma for use in Compton imaging applications.

In order to further all three goals, PIXeY has a unique gas-handling and and cryogenics system for the recirculation of xenon through an external purifier and condensation back into the main volume (Fig. 19). The system that cools and recondenses the xenon consists of two major components. Cooling power is produced by a cold head attached to a liquid nitrogen reservoir. The nitrogen is allowed to boil off at a controlled rate inside the cold head, cooling an array of copper studs that extend down into the main volume where they cool the xenon. In addition, a novel heat exchanger design greatly reduces the cooling power necessary to maintain a steady state inside the detector (Fig. 20). The heat

exchanger consists of a copper pot (the evaporator) situated inside a steel vessel (the condenser) approximately 1 L in volume. Liquid xenon leaving the main volume evaporates inside the evaporator, while gas returning from the purifier enters the condenser and condenses on the vanes on the outer surface of the evaporator, subsequently raining down into the detector. Thus, heat exchange occurs across the copper wall of the evaporator. This design has been tested and shown to reduce the necessary cooling power from 10 W/SLPM to 1.5W/SLPM for circulation rates of up to 22.5 SLPM, corresponding to an 84% efficiency (Fig. 21).
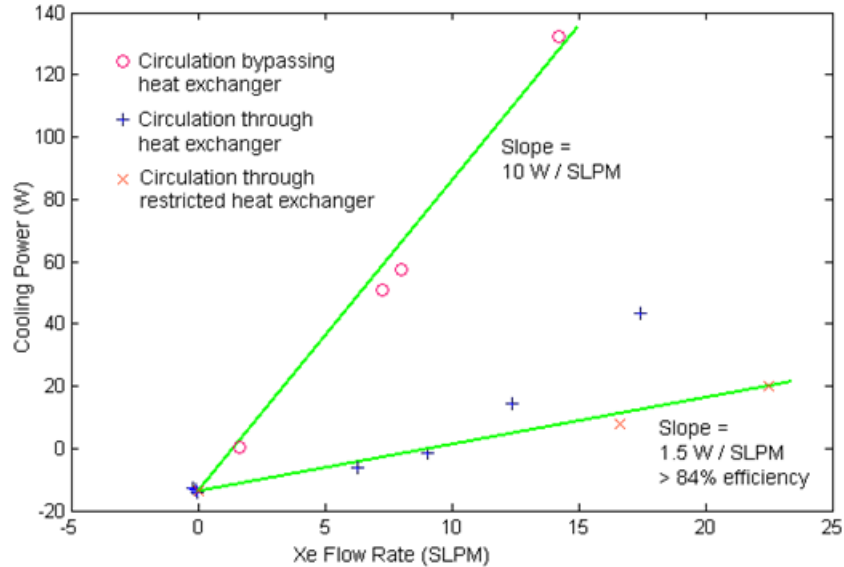

Figure 21: Performance of the PIXeY heat exchanger. Shown here is the cooling power needed to maintain a steady temperature vs. flow rate of the xenon through the external purifier with the heat exchanger in three different configurations (either bypassed, operating normally, or operating with the addition of a flow restrictor). The slope of each line represents the efficiency of each configuration.

3.3   Current Status of PIXeY

Currently, PIXeY is in preparation for its first two-phase run with all systems operational. The internals are completely installed and the circulation system, PMTs, and field grids have all been tested with gaseous xenon. Additionally, calibration data has been taken with both external sources (^{57}Co) and internal sources (^{83m}K), and an analysis framework is in development. Over the next couple weeks, cooldown and condensation will occur, and a campaign to collect two-phase data will begin.

3.4   Specific Involvement

I joined the PIXeY group in June 2009 immediately prior to my first year as a Ph.D student in the Yale Department of Physics. Since then, I have worked on the following aspects of PIXeY experiment:

1. Construction and installation of internals
2. Design, construction, and installation of capacitive liquid level sensors for the xenon volume
3. Characterization of heat exchanger (Special Investigation project for course credit, Spring 2010)
4. Construction and testing of first-generation PMT bases
5. Characterization and health monitoring of PMTs
6. Design of improved second-generation PMT bases

Additionally, I have presented my work on PIXeY at the following professional conferences:

1. APS Fall Meeting 2010 (Oral)

3.5 Future Plans

During the Summer and Fall of 2012, PIXeY will run in two-phase mode. Data will be collected for energy resolution optimization, electric field studies, and track shape studies. The analysis framework will continue to be tested and devloped, work will continue on the design and development of charge readout wires, and the mechanical design for PIXeY's "square" configuration will be completed so that construction on the Compton imager phase of the PIXeY project can begin.
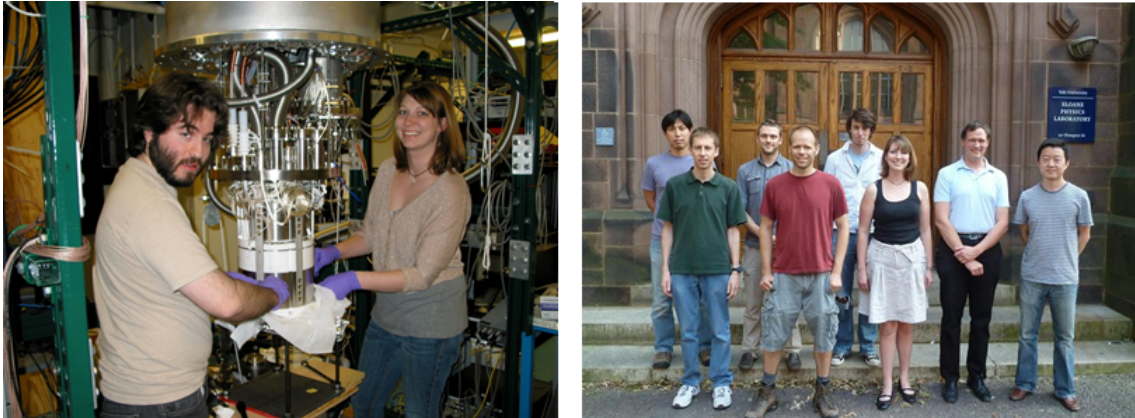

Figure 22: (Left) Installing the PIXeY internals. (Right) The PIXeY collaboration, Fall 2011.

4 Conclusion

In recent years, two-phase xenon time projection chambers have rise to prominence at the forefront of direct dark matter detection and other fundamental physics research. LUX is one such experiment. With a projected sensitivity of 7×10^{46} cm^2, LUX is perfectly poised to either verify or refute the results of recent controversial experiments such as DAMA and COGeNT, which have claimed to see hints of WIMPs in the $\sim$10 GeV mass range [27]. PIXeY is another, smaller-scale xenon-based time projection chamber. Prospects for Compton imaging with PIXeY have been presented, with specific application to the detection of special nuclear materials. Additionally, PIXeY shows great promise with regards to the efficient discrimination between particles (electronic versus nuclear recoils by using charge-to-light ratios, and gammas versus betas by using track shape discrimination) in the detector.

Throughout my time at Yale I have been heavily involved in hardware construction, testing, and design for the LUX and PIXeY experiments. In particular, this includes working on the circulation system and high voltage system for LUX, working on the circulation system, heat exchanger, and PMTs for PIXeY, and operation and monitoring of both detectors during their most recent runs.

I have also presented my work at three different professional conferences, with three more upcoming this year. Additionally, I will be attending the 62nd Lindau Meeting of Nobel Laureates, a prestigious program which brings together twenty-five Nobel Laureates in Physics and 550 students from around the world for one week in Lindau, Germany to exchange ideas and to form valuable networks for the future.

Over the next several months, I will be primarily moving into development of analysis software for both PIXeY and LUX. My ultimate thesis work will center upon one or more of the LUX physics analyses outlined in Section 2.4 as well as particle discrimination and track imaging studies in PIXeY.

References

[1] Zwicky, F. The redshift of extragalactic nebulae. *Helvetic Physica Acta*, vol. 6:(1933) pp. 110–127.

[2] Kahn, F. and Woltjer, L. Intergalactic matter and the galaxy. *The Astrophysical Journal*, vol. 130:(1959) pp. 705–717.

[3] Rubin, V.C. and Ford, W.K. Rotation of the Andromeda nebula from a spectroscopic survey of emission regions. *The Astrophysical Journal*, vol. 159:(1970) pp. 379–403.

[4] Rubin, V.C., Burstein, D., Ford, W.K., and Thonnard, N. Rotation velocities of 16 Sa galaxies and a comparison of Sa, Sb, and Sc rotation properties. *The Astrophysical Journal*, vol. 289:(1985) pp. 81–104.

[5] Wittman, D.M., et al. Detection of weak gravitational lensing distortions of distant galaxies by cosmic dark matter at large scales. *Nature*, vol. 405:(2000) pp. 143–149.

[6] Clowe, D., et al. A direct empirical proof of the existence of dark matter. *The Astrophysical Journal*, vol. 648:(2006) pp. L109–L113.

[7] Jarosik, N., et al. Seven-year Wilkinson Microwave Anisotropy Probe (WMAP) observations: Sky maps, systematic errors, and basic results. *The Astrophysical Journal Supplement Series*, vol. 192.

[8] Hu, W. and Dodelson, S. Cosmic microwave background anisotropies. *Annual Review of Astronomy and Astrophysics*, vol. 40:(2002) pp. 171–216.

[9] Tytler, D., O'Meara, J.M., Suzuki, N., and Lubin, D. Review of Big Bang nucleosynthesis and primordial abundances. *Physica Scripta*, vol. T85:(2000) pp. 12–31.

[10] Kowalski, M., et al. Improved constraints from new, old, and combines supernova datasets. *The Astrophysical Journal*, vol. 686(2):(2008) pp. 749–778.

[11] Blumenthal, G., Faber, S., Primack, J., and Rees, M. Formation of galaxies and large-scale structre with cold dark matter. *Nature*, vol. 311:(1984) pp. 517–525.

[12] Aihara, H., et al. The eigth data release of the Sloan Digital Sky Survey: First data from SDSS-III. *The Astrophysical Journal Supplement Series*, vol. 193.

[13] Bergstrom, L. Dark matter candidates. *New Journal of Physics*, vol. 11.

[14] Battesti, R. Axion searches in the past, at present, and in the near future. *Lecture Notes in Physics*, vol. 741:(2008) pp. 199–237.

[15] Milgrom, M. A modification of the Newtonian dynamics as a possible alternative to the hidden mass hypothesis. *The Astrophysical Journal*, vol. 270:(1983) pp. 365–370.

[16] Sanders, R.H. and McGaugh, S.S. Modified Newtonian dynamics as an alternative to dark matter. *Annual Review of Astronomy and Astrophysics*, vol. 40:(2002) pp. 263–317.

[17] Cirelli, M. Indirect searches for dark matter: A status review. *eprint arXiv:1202.1454*.

[18] Bernabei, R., et al. First results from DAMA/LIBRA and the combined results with DAMA/NaI. *European Physical Journal C*, vol. 56(3):(2008) pp. 333–355.

[19] Ahmed, Z., et al. Dark matter search results from the CDMS II experiment. *Science*, vol. 327(5973):(2010) pp. 1619–1621.

[20] Lewin, J.D. and Smith, P.F. Review of mathematics, numerical factors, and corrections for dark matter experiments based on elastic nuclear recoil. *Astroparticle Physics*, vol. 6:(1996) pp. 87–112.

[21] Boulay, M., Cai, B., and Deap/Clean Collaboration. Dark matter search at SNOLAB with DEAP-1 and DEAP/CLEAN-3600. *Journal of Physics Conference Series*, vol. 136(4).

[22] Manzur, A. *Relative scintillation efficiency of liquid xenon in the XENON10 direct dark matter search.* Ph.D. thesis, 2009.

[23] Aprile, E., et al. Design and performance of the XENON10 dark matter experiment. *Astroparticle Physics*, vol. 34(9):(2011) pp. 679–698.

[24] Ackerman, N., et al. Observation of two-neutrino double-beta decay in ^{136}Xe with the EXO-200 detector. *Physical Review Letters*, vol. 107(21).

[25] Lebedenko, V.N., et al. Results from the first science run of the ZEPLIN-III dark matter search experiment. *Phys. Rev. D*, vol. 80.

[26] Dobi, A., et al. Xenon purity analysis for EXO-200 via mass spectrometry. *Nuclear Instruments and Methods in Physics Research A*, vol. 675:(2012) pp. 40–46.

[27] Cline, D.B. Recent results on the low mass dark matter WIMP controversy: 2011. *eprint arXiv:1109.1799.*